Research Square

Preprints are preliminary reports that have not undergone peer review.
They should not be considered conclusive, used to inform clinical practice,
or referenced by the media as validated information.

Neural-Network Extraction of Nucleon-Nucleon Contact Constants from Phase Shifts

Mayank Goswami

mayankfph@iitr.ac.in

Indian Institute of Technology Roorkee

Gautam Balasubramanian.

Indian Institute of Technology Roorkee

Research Article

Keywords: Inverse scattering, neural networks, nuclear physics, low-energy constants, , Lippmann–Schwinger equation.

Posted Date: November 5th, 2026

DOI: https://doi.org/10.21203/rs.3.rs-11620854/v1

License: This work is licensed under a Creative Commons Attribution 4.0 International License.
Read Full License

Additional Declarations: The authors declare no competing interests.

Neural-Network Extraction of Nucleon-Nucleon Contact Constants from Phase Shifts

Gautam Balasubramanian[1] and Mayank Goswami,[1,2]

[1]Department of Physics, IIT Roorkee
[2]MF School of AI and DS, IIT Roorkee
mayank.goswami@ph.iitr.ac.in

***Abstract*—This work is a neural-network based approach to the inverse scattering of the Nucleon-Nucleon Potential. We infer short-range contact low-energy constants for a truncated model space from phase shifts.**

A simplified interaction model combining one-pion exchange (OPE) and contact interactions is used to generate synthetic scattering data. The forward scattering problem is solved numerically using a discretized Lippmann–Schwinger equation. A multilayer perceptron is trained to map phase-shift data to eight contact LECs.

The network uses 66 input features obtained from six uncoupled partial-wave channels evaluated at eleven energies. A synthetic dataset containing 5,000 parameter samples is generated. The trained network provides initial parameter estimates, which are subsequently refined through bounded least-squares optimization against Nijmegen PWA phase shifts.

The results illustrate the potential of combining neural networks with physics-based optimization. Since the forward model is approximate and omits contributions present in more complete nuclear interactions, the inferred LECs need not coincide with published parameter values. The performance of the method is therefore assessed primarily through parameter recovery and reconstruction of the scattering data. The fitted constants are interpreted as effective parameters within the chosen truncated interaction model and are not taken to demonstrate renormalization or physical equivalence with constants from more complete interactions.

***Index Terms*—Inverse scattering, neural networks, nuclear physics, low-energy constants, , Lippmann–Schwinger equation.**

I. Introduction

The nucleon-nucleon interaction is a fundamental component of nuclear physics. It determines important properties of nuclear systems and is studied experimentally through scattering observables such as differential cross sections and phase shifts.

Chiral effective field theory (EFT) provides a systematic framework for describing nuclear interactions in terms of long-range pion exchange and short-range contact interactions [1, 2, 3, 4].

The strengths of contact interactions are represented by low-energy constants (LECs). These parameters are determined by fitting the theoretical estimates to experimental scattering data.

Corresponding author: mayank.goswami@ph.iitr.ac.in

The conventional extraction of LECs involves repeatedly solving scattering equations and optimizing the parameters. Because the relationship between interaction parameters and scattering observables is non-linear, this procedure can be computationally expensive.

Machine learning provides an alternative approach. A neural network can learn an approximate inverse mapping from scattering observables to interaction parameters using examples generated from a forward physics model. Existing works following similar ideas include [5, 6, 7, 8]

In this project, we investigate a neural-network-assisted inverse-scattering pipeline. A simplified potential model is used to generate synthetic training data. The neural network estimates the contact LECs, and least-squares refinement is subsequently used to improve agreement with reference phase shifts.

The central objective is to investigate whether neural-network predictions can provide useful initial estimates for parameter optimization and whether the approximate model can reproduce the reference scattering observables.

II. Problem Objectives and Motivation

A. The Inverse Scattering Problem

In the scattering problem, an interaction potential is specified and the resulting scattering observables are calculated.

Symbolically, this relationship can be written as

$$\boldsymbol{\delta} = F(\boldsymbol{\theta}), \tag{1}$$

where $\boldsymbol{\theta}$ denotes the vector of contact LECs, $\boldsymbol{\delta}$ denotes the phase-shift data, and F represents the forward scattering calculation.

The inverse problem is to estimate the interaction parameters from the observed phase shifts:

$$\boldsymbol{\theta} \approx F^{-1}(\boldsymbol{\delta}). \tag{2}$$

The inverse mapping need not be unique. Different parameter combinations may produce similar scattering observables over a restricted energy range.

Consequently, recovering the original parameters can be difficult even when the calculated phase shifts agree reasonably well with the reference data.

B. Objectives

The objectives of this project are:

1) Construct a simplified nucleon-nucleon interaction model truncating the complete EMN500 potential to a given order of short and long ranged interaction combining one-pion exchange and contact interactions.
2) Solve the corresponding uncoupled Lippmann–Schwinger equations numerically to obtain the corrected Potential to be used for phase shift calculations.
3) Generate a synthetic dataset containing 5,000 samples of contact parameters using uniform sampling in their specified ranges and their corresponding phase shifts.
4) Train a multilayer perceptron to estimate eight contact LECs from 66 phase-shift input features.
5) Use the network predictions as initial estimates for least-squares refinement against Nijmegen PWA [**Machleidt_2011**] phase shifts.
6) Compare the phase-shift predictions before and after incorporating the LS equation and investigate the limitations caused by the approximate interaction model. Obtain the predicted constants from the model and interpret the results

C. Motivation

Repeatedly solving the scattering problem during parameter optimization (the LECs in this case) can be computationally expensive.

A trained neural network provides a rapid approximation to the inverse mapping and reduces the effort required to obtain useful initial parameter estimates.

The combination of machine learning and conventional optimization is attractive because a fast initial prediction can be followed by physics-based refinement (PINNs) [9].

The motivation is therefore to investigate whether the neural network can assist inverse parameter estimation.

III. Theoretical Framework

A. Nucleon-Nucleon Interaction

In the simplified interaction model, the potential is decomposed into long-range and short-range contributions:

$$V = V_{\mathrm{OPE}} + V_{\mathrm{contact}}. \tag{3}$$

Here, V_{OPE} describes one-pion exchange, while V_{contact} represents short-range interactions parameterized by LECs.

The implemented model is an approximate, truncated interaction rather than a complete higher-order chiral EFT potential.

TABLE I
Partial-wave channels used in the calculation

Channel	L	S	J
$^1S_0$	0	0	0
$^3S_1$	0	1	1
$^1P_1$	1	0	1
$^3P_0$	1	1	0
$^3P_1$	1	1	1
$^3P_2$	1	1	2

B. One-Pion Exchange

The leading momentum-space one-pion-exchange interaction can be expressed schematically as

$$V_{\mathrm{OPE}}(\mathbf{q}) = -\frac{g_A^2}{4f_\pi^2}\frac{(\boldsymbol{\tau}_1\cdot\boldsymbol{\tau}_2)(\boldsymbol{\sigma}_1\cdot\mathbf{q})(\boldsymbol{\sigma}_2\cdot\mathbf{q})}{\mathbf{q}^2+m_\pi^2}, \tag{4}$$

where g_A is the axial coupling, f_π is the pion decay constant, m_π is the pion mass, and $\boldsymbol{\sigma}_i$ and $\boldsymbol{\tau}_i$ are spin and isospin Pauli matrices.

The momentum transfer is

$$\mathbf{q} = \mathbf{p}' - \mathbf{p}. \tag{5}$$

The denominator describes the finite range associated with pion exchange, while the spin and isospin operators determine the channel dependence of the interaction.

The constants used in the implementation are

$$m_\pi = 138.0 \text{ MeV}, \tag{6}$$
$$M_N = 938.92 \text{ MeV}, \tag{7}$$
$$g_A = 1.29, \tag{8}$$
$$f_\pi = 92.4 \text{ MeV}. \tag{9}$$

C. Channel-Wise OPE

The interaction must be projected onto states with definite orbital angular momentum L, total spin S, total angular momentum J, and isospin T. Moreover, our phase shift data is also channel-wise provided so this analysis has to be performed.

The partial-wave matrix element is written schematically as

$$V_{L'L}^{JST}(p',p) = \langle p', L'SJ,T|V_{\mathrm{OPE}}|p,LSJ,T\rangle\,. \tag{10}$$

The projection accounts for the angular dependence and spin structure of the interaction. In the implementation, the angular integrals and spin-angular coefficients are evaluated numerically.

For two nucleons, the isospin factor is

$$\langle\tau_1\cdot\tau_2\rangle = 2\cdot T(T+1) - 3 \tag{11}$$

$$\boldsymbol{\tau}_1\cdot\boldsymbol{\tau}_2 = \begin{cases} -3, & T=0, \\ +1, & T=1. \end{cases} \tag{12}$$

The six channels considered are listed in Table I.

The ${}^1S_0$ channel has $T = 1$, whereas the ${}^3S_1$ channel has $T = 0$. The four P-wave channels have $T = 1$.

The different quantum numbers produce different OPE matrix elements across the channels.

An important approximation is made in the triplet S-wave. The physical ${}^3S_1$ state is coupled to ${}^3D_1$ through the tensor interaction. The present calculation treats ${}^3S_1$ as uncoupled and therefore treats only the uncoupled block.

D. Short-Range Contact Interactions

The short-range interaction is parameterized using momentum-dependent contact terms.

For the S-wave channels, the implemented interaction is

$$V^S_{\rm contact}(p',p) = \widetilde{C}_S f_3(p',p) + C_S(p'^2+p^2) f_2(p',p). \tag{13}$$

Here, $\widetilde{C}_S$ and C_S are the two contact LECs associated with the relevant S-wave channel.

For the P-wave channels, the contact interaction is

$$V^P_{\rm contact}(p',p) = C_P p' p\, f_2(p',p), \tag{14}$$

where C_P is the corresponding P-wave LEC.

The regulator is

$$f_n(p',p) = \exp\left[-\left(\frac{p'}{\Lambda}\right)^{2n} - \left(\frac{p}{\Lambda}\right)^{2n}\right], \tag{15}$$

with cutoff

$$\Lambda = 500 \text{ MeV}. \tag{16}$$

The implementation uses $n = 3$ for the zero-order S-wave contact terms and $n = 2$ for the momentum-dependent terms and P-wave contacts.

The regulator suppresses contributions from momenta much larger than the chosen cutoff. The LECs determine the strength of the short-range interaction within this regulated model. A regulator is necessary to ensure the Lippman-Schwinger equation is properly solved.

Their numerical values depend on the regulator, operator basis, long-range interaction, and fitting data.

E. The Lippmann–Schwinger Equation

The scattering amplitude satisfies the Lippmann–Schwinger equation

$$T(\mathbf{p}',\mathbf{p}) = V(\mathbf{p}',\mathbf{p}) + \int \frac{d^3q}{(2\pi)^3} V(\mathbf{p}',\mathbf{q}) \frac{1}{E - H_0(q) + i0^+} T(\mathbf{q},\mathbf{p}). \tag{17}$$

Here, V is the interaction potential, T is the scattering amplitude, H_0 is the free Hamiltonian, and E is the scattering energy.

The equation accounts for repeated interactions between the two nucleons.

For an uncoupled partial wave, a principal-value formulation of the real reaction matrix R can be written as

$$R(p',p) = V(p',p) + \mathcal{P}\int dq\, q^2 V(p',q) \frac{M_N}{p^2_{\rm on} - q^2} R(q,p), \tag{18}$$

where $p_{\rm on}$ is the on-shell momentum and $\mathcal{P}$ denotes the principal-value prescription.

The exact normalization factors depend on the partial-wave convention used by the solver.

For the nonrelativistic kinematics implemented in the code,

$$p_{\rm on} = \sqrt{\frac{M_N E_{\rm lab}}{2}}. \tag{19}$$

F. Numerical Solution of the LS Equation

The momentum integral is discretized using Gauss–Legendre quadrature with 48 quadrature points. An additional on-shell point is included to evaluate the reaction matrix at the physical scattering momentum. This method is based on [10].

The singularity at $q = p_{\rm on}$ is handled using a subtraction procedure, which modifies the numerical weights and adds a correction term.

After discretization, the reaction-matrix equation takes the form

$$R_{ij} = V_{ij} + \sum_k V_{ik} D_k R_{kj}, \tag{20}$$

where D_k contains the quadrature weights, momentum factors, propagator denominator, and subtraction correction.

In matrix notation,

$$(I - VD)R = V. \tag{21}$$

The required reaction-matrix column is obtained by solving the resulting linear system.

The on-shell reaction matrix is then converted into a phase shift using the normalization adopted in the code:

$$\tan\delta = -\frac{\pi}{2} \frac{M_N p_{\rm on}}{(2\pi)^3} R(p_{\rm on}, p_{\rm on}). \tag{22}$$

The resulting phase shifts are converted to degrees. Phase-shift branches must be handled consistently because the principal arctangent returns values between $-90°$ and $90°$, while physical phase shifts may lie outside this interval.

The implementation also applies a branch correction in the triplet S-wave associated with the deuteron and Levinson's theorem.

The normalization and branch conventions must be consistent with those used for the reference phase shifts.

IV. Previous Work

A. Nuclear Interactions and Chiral EFT

Chiral EFT provides a systematic framework for nuclear interactions through an expansion in characteristic momenta and the pion mass relative to a breakdown scale.

Long-range pion-exchange terms and short-range contact operators enter at different orders.

Machleidt and Entem reviewed the theoretical development of chiral nuclear forces and their application to nucleon-nucleon scattering [1].

Entem, Machleidt, and Nosyk developed high-quality nucleon-nucleon potentials through fifth order of the chiral expansion. Such interactions include contributions not present in the simplified model considered here.

B. Nijmegen Phase-Shift Analysis

Nijmegen PWA93 provides a partial-wave analysis of nucleon-nucleon scattering data below 350 MeV [11].

The resulting phase shifts provide reference values for comparing theoretical interaction models with scattering information. A procedure as such is described in the review [12]

In this project, Nijmegen PWA93 phase shifts are used as targets in the final parameter-refinement stage.

C. Machine Learning for Inverse Problems

Neural networks can approximate non-linear mappings between observables and model parameters.

In this project, the network learns from synthetic data generated by a forward scattering solver. It provides initial parameter estimates, which are then refined using a conventional optimization algorithm.

The network is therefore used as an approximate inverse map rather than as a replacement for the underlying scattering calculation.

V. Methodology

A. Generation of Synthetic Data

Eight contact LECs are varied within prescribed sampling ranges. For every sampled parameter vector, the forward solver calculates phase shifts in six uncoupled channels.

A synthetic dataset containing 5,000 randomly generated parameter samples is constructed.

The LEC sampling ranges used in the implementation are listed in Table II.

The forward solver uses the energy grid

$$E_{\mathrm{lab}} = [1, 5, 10, 40, 70, 100, 130, 160, 190, 220, 250, 280, 300]\ \mathrm{MeV}. \tag{23}$$

The 1 MeV and 5 MeV points serve as additional low-energy anchors and are not included in the neural-network input.

The network receives phase shifts at eleven energies for each of the six channels. Therefore,

TABLE II
LEC sampling ranges used in the implementation

LEC	Sampling range
$\widetilde{C}_{1S0}$	$[-1.5, 1.5]$
C_{1S0}	$[-6, 6]$
$\widetilde{C}_{3S1}$	$[-1.5, 1.5]$
C_{3S1}	$[-6, 6]$
C_{1P1}	$[-3, 3]$
C_{3P0}	$[-3, 3]$
C_{3P1}	$[-3, 3]$
C_{3P2}	$[-3, 3]$

$$N_{\mathrm{input}} = 6 \times 11 = 66. \tag{24}$$

The output consists of the eight contact LECs.

B. Neural-Network Architecture

The inverse mapping is approximated using a multilayer perceptron implemented in PyTorch.

The architecture is

$$66 \longrightarrow 128 \longrightarrow 64 \longrightarrow 8. \tag{25}$$

The hidden layers use rectified linear unit activations:

$$\mathrm{ReLU}(x) = \max(0, x). \tag{26}$$

The network receives 66 phase-shift features and predicts the eight contact parameters.

C. Data Preprocessing and Training

The dataset is divided into training, validation, and test subsets using a 70:15:15 split.

StandardScaler is fitted separately to the training inputs and training targets. The transformations are then applied to the validation and test subsets.

The training objective is the mean squared error:

$$\mathcal{L}_{\mathrm{MSE}} = \frac{1}{N} \sum_{i=1}^{N} \left\| \widehat{\boldsymbol{\theta}}_i - \boldsymbol{\theta}_i \right\|_2^2, \tag{27}$$

where the network predictions and targets are expressed in standardized target coordinates during training.

The main training settings are:

- Optimizer: Adam.
- Learning rate: 10^{-3}.
- Weight decay: 10^{-5}.
- Batch size: 32.
- Number of epochs: 1000.
- Hidden-layer activation: ReLU.

D. Inference on Nijmegen Phase Shifts

After training, the Nijmegen PWA93 phase shifts are organized into the same 66-feature ordering used for the synthetic training data.

The trained network provides an initial estimate:

$$\boldsymbol{\theta}_{\mathrm{NN}} = \mathcal{N}_{\mathrm{trained}}(\boldsymbol{\delta}_{\mathrm{PWA93}}). \tag{28}$$

The predicted LECs are then passed through the forward solver to calculate the corresponding phase shifts.

E. Least-Squares Refinement

The neural-network estimates are used as initial parameters for least-squares optimization.

The objective is to minimize the difference between calculated and reference phase shifts:

$$\boldsymbol{\theta}_{\mathrm{ref}} = \arg\min_{\boldsymbol{\theta}} \sum_{i=1}^{N_E} \left[\mathrm{wrap}\left(\delta_{\mathrm{calc}}(E_i;\boldsymbol{\theta}) - \delta_{\mathrm{ref}}(E_i)\right)\right]^2 . \tag{29}$$

Here, $N_E = 11$, and the wrapping function accounts for the 180° periodicity of the phase-shift branch.

Each channel is refined independently in the implementation. The two S-wave channels have two associated LECs each, whereas each P-wave channel has one contact LEC.

The SciPy `least_squares` routine is used with parameter bounds and multiple initial estimates. The candidate with the smallest residual cost is retained.

The complete computational pipeline is

$$\boxed{\begin{array}{c}\text{Sample LECs} \rightarrow \text{Construct potential} \\ \rightarrow \text{Solve LS equation} \rightarrow \text{Generate phase shifts} \\ \rightarrow \text{Train neural network} \rightarrow \text{Predict LECs} \\ \rightarrow \text{Least-squares refinement} \rightarrow \text{Compare phase shifts.}\end{array}} \tag{30}$$

VI. Results

A. Synthetic Test-Set LEC Recovery

The trained network is evaluated on a held-out synthetic test set to examine how accurately it recovers individual contact LECs.

The coefficient of determination is calculated separately for each parameter:

$$R^2 = 1 - \frac{\sum_i (\theta_i - \widehat{\theta}_i)^2}{\sum_i (\theta_i - \overline{\theta})^2}. \tag{31}$$

Here, θ_i denotes the true synthetic test-set parameter, $\widehat{\theta}_i$ is its prediction, and $\overline{\theta}$ is the mean of the true values.

Figure 1 shows that the network's parameter recovery performance depends on the LEC.

Several P-wave contact parameters exhibit high R^2 values, whereas the zero-order S-wave constants show weaker recovery. The relatively lower score for $\widetilde{C}_{3S1}$ suggests that this parameter is more difficult to infer from the selected phase-shift features.

This behavior may reflect differences in parameter sensitivity and identifiability. Different combinations of contact parameters may generate similar phase shifts over the finite energy grid.

These R^2 values measure recovery on the synthetic test set. They do not directly measure agreement with the true LECs of the Nijmegen interaction.

B. Extracted Contact LECs

The network predictions are used as initial estimates for the least-squares refinement stage.

Figure 2 compares the LEC estimates before and after refinement. Several parameters change substantially, indicating that the network predictions act primarily as initial estimates for the subsequent optimization.

The refined values are determined by the forward model, reference phase shifts, optimization objective, and parameter bounds.

Because the implemented interaction is approximate, the resulting LECs should be interpreted as effective parameters within the model. They should not be assumed to coincide with published constants from a more complete nuclear interaction.

C. Phase-Shift Reconstruction

The principal physical test of the fitted parameters is whether the calculated phase shifts reproduce the reference scattering observables.

Figure 3 compares the calculated phase shifts with the Nijmegen PWA93 reference data.

The initial neural-network predictions exhibit substantial discrepancies in the ${}^1S_0$ and ${}^3S_1$ channels. Following least-squares refinement, the calculated curves show substantially improved agreement with the reference points.

The ${}^1P_1$ channel exhibits close agreement between the refined predictions and the reference data. The ${}^3P_0$ and ${}^3P_1$ channels also show improved agreement, although residual differences remain.

In the ${}^3P_2$ channel, the refined curve does not reproduce all reference points exactly, particularly at intermediate and higher energies.

These results illustrate the benefit of combining neural-network inference with conventional optimization. However, the remaining discrepancies also indicate the limitations of the approximate interaction model.

A quantitative assessment should include channel-by-channel phase-shift errors before and after refinement, rather than relying exclusively on visual agreement.

D. Why the Extracted LECs Differ from Reference Values

The inferred LECs need not coincide with published values associated with Nijmegen-related or EMN interactions.

The reference Nijmegen PWA93 phase shifts are obtained from a partial-wave analysis of scattering data, whereas the present forward simulator uses a simplified potential.

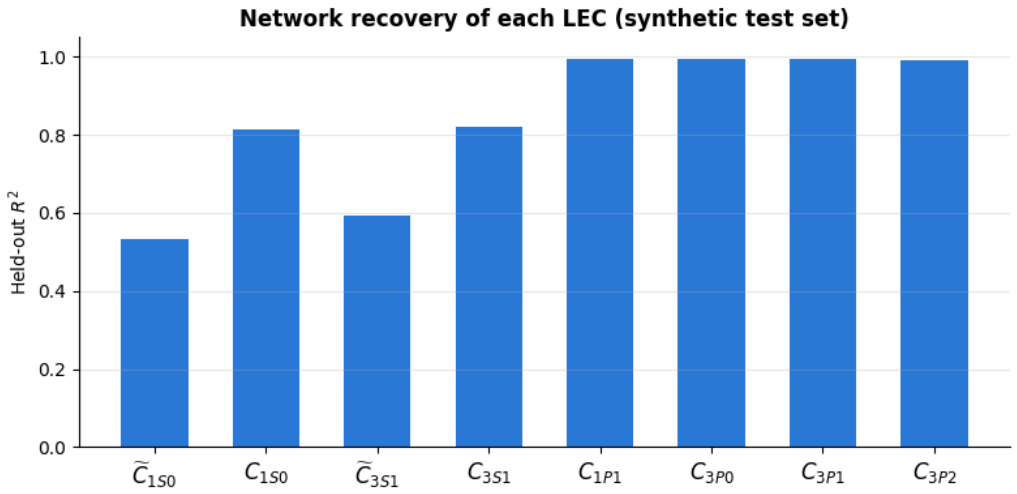


Fig. 1. Coefficient of determination (R^2) for individual contact LEC predictions on the held-out synthetic test set. The variation across parameters indicates differences in parameter recovery performance.

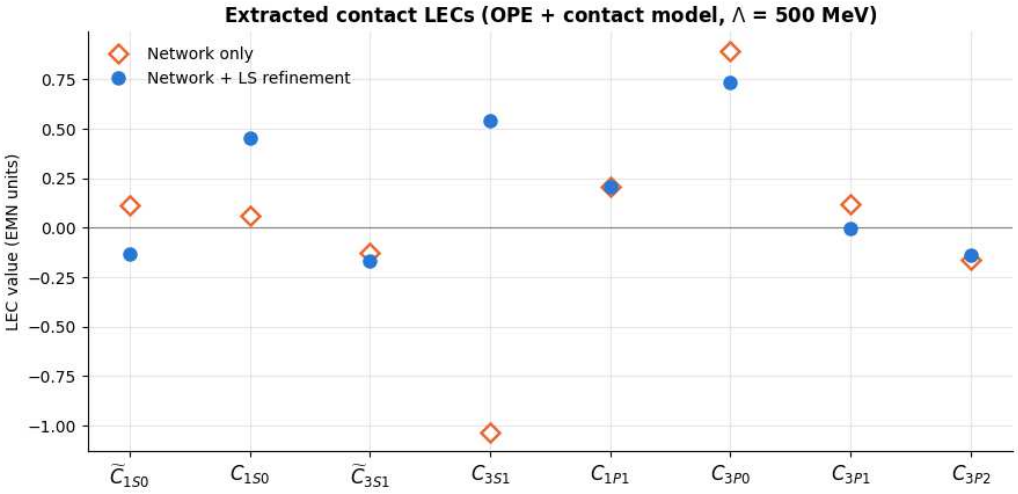


Fig. 2. Contact LEC estimates obtained from the neural network before and after least-squares refinement using the OPE-plus-contact model with a cutoff of $\Lambda = 500\,\mathrm{MeV}$.

The model includes OPE and a restricted set of contact terms, but omits important contributions present in more complete nuclear interactions, including the full two-pion-exchange contributions of higher-order chiral EFT.

Furthermore, the physical ${}^3S_1$ channel is coupled to ${}^3D_1$ through the tensor force, whereas the present calculation treats the channels as uncoupled.

The fitted contact parameters may therefore compensate for discrepancies between the approximate interaction and the reference scattering data.

This is consistent with the role of effective parameters in approximate models. However, it does not by itself establish that the fitted constants are physically equivalent to the reference LECs.

Differences may also arise from the regulator, operator normalization, parameter bounds, and finite energy grid.

E. Parameter Accuracy Versus Observable Accuracy

Parameter accuracy and observable accuracy are distinct.

Parameter accuracy concerns agreement between predicted LECs and known parameter values:

$$\epsilon_{\mathrm{LEC}} = \|\boldsymbol{\theta}_{\mathrm{pred}} - \boldsymbol{\theta}_{\mathrm{reference}}\|\,. \tag{32}$$

Observable accuracy concerns agreement between predicted and reference phase shifts:

$$\mathrm{RMSE}_\delta = \sqrt{\frac{1}{N_E}\sum_{i=1}^{N_E}[\delta_{\mathrm{pred}}(E_i) - \delta_{\mathrm{ref}}(E_i)]^2}. \tag{33}$$

For an approximate interaction model, good observable agreement does not necessarily imply exact recovery of the original LECs.

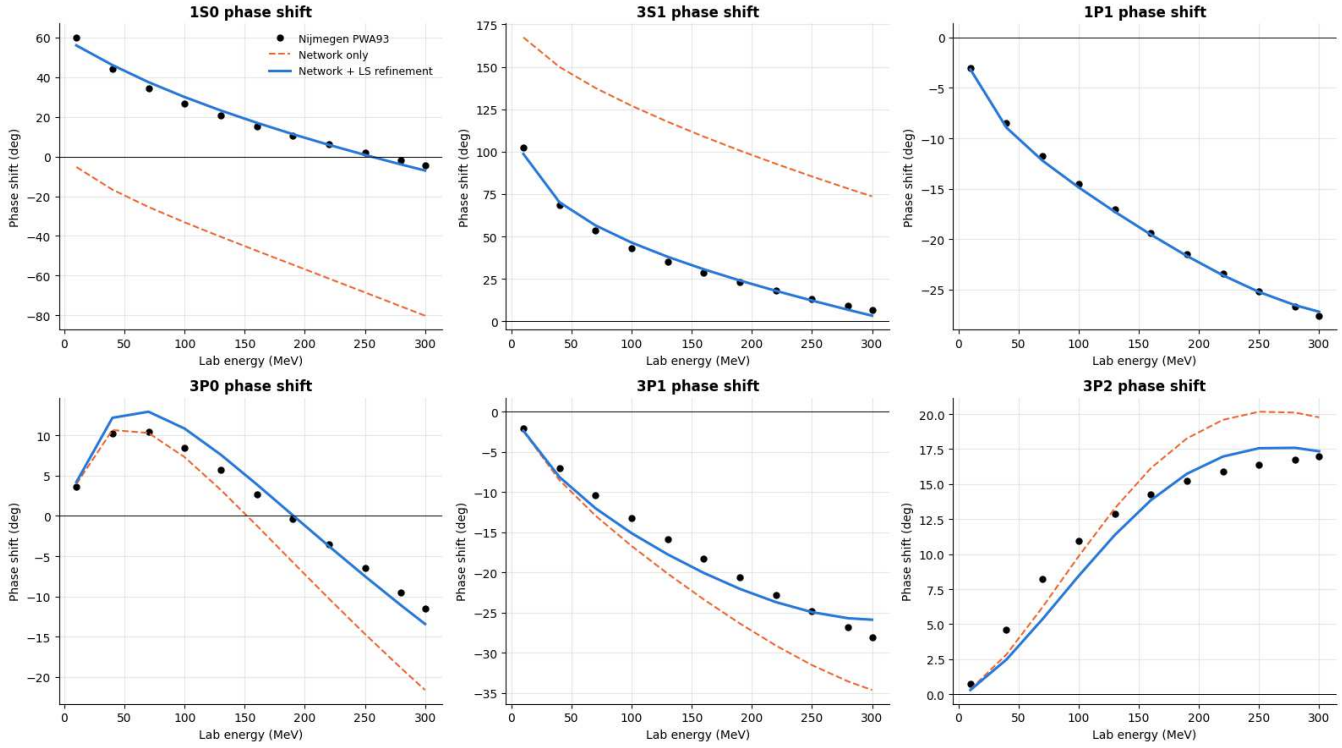


Fig. 3. Phase shifts as functions of laboratory energy for six uncoupled partial-wave channels. Black points represent Nijmegen PWA93 reference data, orange dashed curves show neural-network predictions, and blue curves show predictions after least-squares refinement.

Phase-shift reconstruction is therefore an essential performance measure for the present method, although agreement at the fitted energies does not guarantee accurate predictions outside that range.

VII. Conclusion

A neural-network-assisted inverse-scattering method has been investigated using a simplified OPE-plus-contact nuclear interaction model.

The forward scattering problem is solved using a discretized Lippmann–Schwinger equation, and synthetic phase-shift data are used to train a multilayer perceptron that maps 66 input features to eight contact LECs.

The network provides initial estimates for the Nijmegen PWA93 phase shifts. These estimates are subsequently refined through least-squares optimization.

The synthetic test-set results indicate that parameter recovery depends on the individual LEC. The phase-shift comparisons show that refinement improves agreement with the reference data in several channels, although residual discrepancies remain.

Differences between inferred and published LECs are consistent with the limitations of an approximate interaction model and the possible non-uniqueness of the inverse problem. They should not automatically be interpreted as evidence of exact parameter recovery.

Overall, the project demonstrates a computational framework combining neural-network inference and numerical optimization. Further validation is required to establish the robustness and computational advantages of the method.

VIII. Limitations

A. Approximate Interaction Model

The model combines OPE with a restricted set of contact interactions. It does not include all contributions present in a complete higher-order chiral interaction.

The contact parameters may therefore compensate for omitted physics and do not agree with standard EMN LECs.

B. Uncoupled-Channel Approximation

The physical $^3S_1$ channel is coupled to $^3D_1$ through the tensor interaction. The present implementation treats the $^3S_1$ channel independently and omits this coupling.

This approximation limits the model's ability to reproduce the full physics of the triplet coupled-channel.

C. Finite Energy Grid

The neural network uses phase shifts at eleven laboratory energies between 10 and 300 MeV. The 1 MeV and 5 MeV points are used by the forward solver but are not network inputs.

The finite input grid may limit the information available for distinguishing parameter combinations that produce similar phase shifts.

D. Inverse-Problem Non-Uniqueness

Different LEC combinations may produce similar phase shifts within the selected model and energy range. Consequently, the inverse mapping may not uniquely determine the original parameters.

A small phase-shift error therefore does not necessarily imply that the inferred LECs match those of a more complete interaction.

E. Neural-Network Generalization

The synthetic test-set results vary across individual LECs. Some parameters are recovered more accurately than others, suggesting that parameter sensitivity and identifiability are important limitations.

Early stopping, regularization, and broader training-data coverage could be investigated to improve generalization.

F. Optimization Dependence

The final results depend on the least-squares objective, parameter bounds, and starting estimates. Different initial conditions may converge to different minima.

The refinement bounds should be checked to ensure that they match the intended LEC sampling ranges.

G. Reference-Data and Model Consistency

The synthetic training data are generated using the approximate forward model, whereas the final target is the Nijmegen PWA93 phase-shift analysis.

Differences between these sources introduce a model mismatch that limits how accurately the network can infer parameters using the synthetic training data.

H. Future Work

Future work should include coupled-channel calculations, more complete long-range interactions, quantitative channel-by-channel error analysis, and independent validation of the complete pipeline.

Parameter uncertainty and identifiability should also be investigated. Finally, the computational cost of neural-network-assisted optimization should be compared with conventional least-squares fitting from multiple initial conditions.

This work demonstrates the ability of a Neural Network to learn the non-linear scattering space dynamics without biased training data.

IX. Video Resource

https://youtu.be/AG0xuBfWmqs

References

[1] R. Machleidt and D. R. Entem. "Chiral effective field theory and nuclear forces". In: *Physics Reports* 503.1 (2011), pp. 1–75. DOI: 10.1016/j.physrep.2011.02.001.

[2] D. R. Entem, R. Machleidt, and Y. Nosyk. "High-quality two-nucleon potentials up to fifth order of the chiral expansion". In: *Physical Review C* 96 (2017), p. 024004. DOI: 10.1103/PhysRevC.96.024004.

[3] D. R. Entem and R. Machleidt. "Accurate nucleon-nucleon potential based upon chiral perturbation theory". In: *Physical Review C* 68 (2003), p. 041001. DOI: 10.1103/PhysRevC.68.041001.

[4] Evgeny Epelbaum, Hans-Werner Hammer, and Ulf-G. Meißner. "Modern theory of nuclear forces". In: *Reviews of Modern Physics* 81.4 (2009), pp. 1773–1825. DOI: 10.1103/RevModPhys.81.1773.

[5] G. Balassa. "Fixed-energy inverse scattering with radial basis function neural networks and its application to neutron–alpha interactions". In: *Progress of Theoretical and Experimental Physics* 2023.11 (2023), 113A01. DOI: 10.1093/ptep/ptad131.

[6] G. Balassa. "Estimating scattering potentials in inverse problems with Volterra series and neural networks". In: *The European Physical Journal A* 58 (2022), p. 186. DOI: 10.1140/epja/s10050-022-00839-y.

[7] K. Raghavan et al. "Machine-learning-based inversion of nuclear responses". In: *Physical Review C* 103 (2021), p. 035502. DOI: 10.1103/PhysRevC.103.035502.

[8] J. Brehmer et al. "A guide to constraining effective field theories with machine learning". In: *Physical Review D* 98 (2018), p. 052004. DOI: 10.1103/PhysRevD.98.052004.

[9] Maziar Raissi, Paris Perdikaris, and George E. Karniadakis. "Physics-informed neural networks: A deep learning framework for solving forward and inverse problems involving nonlinear partial differential equations". In: *Journal of Computational Physics* 378 (2019), pp. 686–707. DOI: 10.1016/j.jcp.2018.10.045.

[10] Michael I. Haftel and Frank Tabakin. "A matrix inversion method for the Lippmann-Schwinger equation". In: *Nuclear Physics A* 203.2 (1973), pp. 333–352. ISSN: 0375-9474. DOI: 10.1016/0375-9474(73)90430-8. URL: https://sciencedirect.com.

[11] V. G. J. Stoks et al. "Partial-wave analysis of all nucleon-nucleon scattering data below 350 MeV". In: *Physical Review C* 48.2 (1993), pp. 792–815. DOI: 10.1103/PhysRevC.48.792.

[12] R. Navarro Pérez, J. E. Amaro, and E. Ruiz Arriola. "Coarse-grained potential analysis of neutron-proton and proton-proton scattering below the pion production threshold". In: *Physical Review C* 88.6 (2013), p. 064002. DOI: 10.1103/PhysRevC.88.064002.